Fibers and Polymers
https://doi.org/10.1007/s12221-024-00823-x

Online ISSN 1875-0052
Print ISSN 1229-9197

REGULAR ARTICLE

Enhancing Nitric Oxide Gas Detection by Tuning the Structural Dimension of Electrospun ZnO Nanofibers Fibers and Polymers

Niloufar Khomarloo[1,3,5] · Hayriye Gidik[2,4] · Roohollah Bagherzadeh[1] · Masoud Latifi[5] · Marc Debliquy[7] · Ahmadou Ly[6] · Driss Lahem[6] · Elham Mohsenzadeh[2,4]

Received: 17 August 2024 / Revised: 16 November 2024 / Accepted: 20 November 2024

Abstract

We report a systematic investigation into the optimization of ZnO nanofiber-based NO gas sensors through precise control of structural parameters. By employing electrospinning technique, we fabricated ZnO nanofibers with controlled diameters (160–310 nm) and thicknesses (19–25 µm), enabling detailed analysis of structure–property relationships in gas sensing performance. The sensors exhibited optimal performance at 200 °C operating temperature, with the thinnest membrane (160 µm) and smallest fiber diameter (9.52 µm) demonstrating superior sensing capabilities. Under these optimized conditions, the sensor achieved a remarkable sensitivity of 25 (Ω/Ω) toward 500 ppb NO gas with a notably fast recovery time of 191 s. Structural characterization revealed that reducing membrane thickness by 30% enhanced sensitivity by 96%, attributed to increased pore area accessibility. In addition, decreasing nanofiber diameter by 90% resulted in a twofold improvement in NO gas sensitivity. The sensing mechanism was elucidated through energy band analysis, revealing the critical role of electron depletion layer modulation at the gas–solid interface. The sensors demonstrated excellent selectivity against common interferents including ethanol, isopropanol, and acetone, with NO response approximately 84 times greater than these compounds. This study provides crucial insights into the rational design of metal oxide nanofiber architectures for enhanced gas sensing performance, offering potential applications in both industrial and biomedical monitoring systems.

Keywords Nitric oxide (NO) · Electrospun nanofibers · Zinc oxide (ZnO) · Sensor structure · Sensor thickness · Nanofiber diameter

1 Introduction

Nitric oxide (NO) is a harmful gas produced in the form of by-products of industrial production and combustion. It not only is one of the important sources of acid rain, but also destroys the olfactory oxygen layer [1]. Moreover, it can react with water and oxygen on the skin, in the eyes and mucosa, and eventually turn into irritant substances, namely nitric acid and nitrite, which harm human health [1]. In addition, the increase of NO level in exhaled breath can be a sign of respiratory disease [2, 3]. Aside from medical application, NO is a typical air pollutant exhausting from car engines, boilers or any other combustion processes on every basis. Nonetheless, low-cost NO detectors for distributed ambient sensors and point-of-care applications are lacking. Therefore, developing a gas sensor to detect NO gas in industrial and biomedical applications is a matter of importance.

Recent advances in NO gas sensing have highlighted the critical importance of developing highly sensitive

✉ Roohollah Bagherzadeh
bagherzadeh_r@aut.ac.ir

1 Advanced Fibrous Materials Lab (AFM-LAB), Institute for Advanced Textile Materials and Technology, Amirkabir University of Technology (Tehran Polytechnic), Tehran, Iran

2 Université de Lille, ENSAIT, Laboratoire Génie Et Matériaux Textile (GEMTEX), 59000 Lille, France

3 Université de Lille, ENGYSYS, Lille, France

4 Junia, 59000 Lille, France

5 Textile Engineering Department, Textile Research and Excellence Centers, Amirkabir University of Technology (Tehran Polytechnic), Tehran, Iran

6 Sensors Unit, Materia Nova ASBL, 56 Rue de L'Epargne, 7000 Mons, Belgium

7 Materials Science Department, UMONS, 56, Rue de L'Epargne, 7000 Mons, Belgium

Published online: 22 December 2024

and selective detection methods. For instance, innovative approaches using surface plasmon resonance (SPR) coupled with 2D materials have demonstrated remarkable NO detection capabilities down to parts-per-billion levels while operating at room temperature. These developments underscore the diverse strategies being explored for NO detection, ranging from optical to conductometric approaches, particularly the recent advances in functionalized sensing materials that can achieve selective NO detection even in complex gas mixtures, which is crucial for both environmental monitoring and medical diagnostics applications. The development of nanomaterial-based gas sensors has significantly excelled in recent years by employing different approached so as to enhance sensitivity and selectivity. Among these, the incorporation of noble metal nanoparticles and the development of hierarchical nanostructures have shown promising results in improving gas sensing performance. Recent studies have demonstrated that modified sensing materials, particularly those incorporating precise structural engineering at the nanoscale, can considerably increase gas molecule adsorption and subsequent charge transfer processes, leading to improved sensor response and recovery times.

To address this, semiconductor metal oxide (SMO) sensors occupy a significant part of the gas sensor component market. While there are many approaches available for gas detection, metal oxide sensors remain to be widely used for a range of gas species as they have gained significant research attention owing to their advantages, such as portability, fast operation, low cost and power consumption, and ease of integration [4]. These devices have the merits of being low cost, highly sensitive, fast responding as well as relatively simple, which are beneficial when encountering new applications, especially in portable devices [5]. To date, a variety of semiconductors have been used to construct gas sensors, including SnO_2 [6–9], In_2O_3 [10–12], ZnO [13–16], TiO_2 [17]. Among them, ZnO is often used as a gas sensitive material for preparing NO gas sensors [14, 16]. ZnO (zinc oxide) is a typical n-type semiconducting metal oxide being low cost and environment friendly as well as having high exciton binding energy, 3.37 eV wide band gap, and high electron mobility [1]. It has been extensively used in gas sensing devices due to its low production costs and non-toxic property. ZnO with nanostructure is particularly promising [18] because the large surface-to-volume ratio enhances the sensitivity [15].

The operation basis of resistive type sensors is based on changes in resistance (or conductance) of the gas sensing material as induced by the surrounding gas. The changes are caused by various processes, which can take place both at the surface and in the bulk of gas sensing material [5]. Thus, the structure of sensing layer holds significance in SMO-based gas sensors due to their general mechanism.

Previously documented methods for depositing the sensing layer include magnetron sputtering [5], sol–gel [6], chemical vapor deposition (CVD) [7], ultrasonic spray pyrolysis [5] and electrospinning [19]. By employing the electrospinning technique followed by calcination, ZnO can be transformed into nanofibers, leading to enhanced gas sensor performance. The high aspect ratio, surface-area-to-volume ratio, and the ability to create diverse nanostructures and controlled shapes contribute significantly to improved sensing capabilities [16]. There are numerous possible electrospinning parameters, controlling the structure of nanofibers [20]. In previous researches, various nanofiber structures have been produced, including hollow [21–23], core–shell [24], and composite configurations [18, 25]. To investigate the impact of structural characteristics on sensing performance, several modifications were made to SMO structures. In the study by Choi et al. [26], ZnO nanofiber-based NO_2 sensors were developed and compared to conventional thin-film ZnO-based gas sensors. The findings indicated that the nanofiber-based NO_2 sensors exhibited a significantly higher and faster response at 350 °C. This improvement in performance was attributed to the porous structure of the nanofibers, which displayed a heightened sensitivity to the gas. Similarly, Katoch et al. found that hollow ZnO nanofibers with smaller hole diameters demonstrated higher sensitivity to reducing and oxidizing gases compared to their larger diameter counterparts [22]. Furthermore, in a separate study, core–shell electrospun polycrystalline ZnO demonstrated a strong response to NO_2 [27]. It is important to note that the sensitivity of sensors fabricated using thick film technology is also influenced by the film thickness. In this regard, various authors have reported significantly different dependencies between sensitivity and film thickness in their studies. This is especially significant given that sensing membrane thickness exerts contrasting effects on the detection of different gases, depending on whether they are oxidizing or reducing agents [5]. For instance, increasing nanofiber membrane thickness results in a reduced response to ozone [28] gas but an enhanced response to hydrogen gas [29]. This disagreement underscores complicated gas sensing of metal oxides, since it depends on multiple challenging factors. The depth of gas penetration into the oxide matrix is intricately linked to the diffusion coefficient and activity of the specific gases [30].

Overall, none of these studies focus on the changing the thickness and diameter of electrospun ZnO nanofibers for the improvement of sensitivity and response/recovery time of NO gas. Therefore, this study addresses the challenging task of detecting NO gas, highlighting its vital contribution to the field by analyzing the gas mechanism through varying the thickness of the as-spun membrane in addition to adjusting the diameter of the calcinated nanofibers thorough altering the electrospinning parameters.

To accomplish this, ZnO nanofibers with three different diameters and three distinct thicknesses were synthesized using the electrospinning method, with adjustments made to the voltage, distance, and surface area of the collector. Subsequently, the prepared sensors were tested at the optimal operating temperature of 200 °C, evaluating their performance across various gas concentrations. Remarkably, the sensors displayed a highly promising low-temperature NO gas sensing performance, particularly in the case of the thinner membrane and the lowest nanofiber diameter (measuring 160 um and 9.52 um, respectively). The sensor exhibited an exceptional response magnitude, reaching a value of 22 when exposed to 500 ppb of NO gas concentration, which, to the best of our knowledge, surpasses previous reported results. Furthermore, the potential sensing mechanism has been explained in this study through the use of an energy band diagram, providing insight on the underlying processes.

2 Materials and Methods

2.1 Synthesizing ZnO Nanofibers

Defined polyvinyl alcohol (PVA) and zinc acetate ($Zn(CH_3CO_2)_2$) (ZnAc) were obtained from Sigma-Aldrich. Porous ZnO nanofibers were synthesized by electrospinning technique using an electrospinning cabin (Fluidnatek/LE 50, Bioinicia, Spain). To do so, zinc acetate and polyvinyl alcohol with the ratio of ZnAc:PVA = 1.5 was prepared in distilled water (DW). First, ZnAc and DW dispersion followed by ultrasonic was performed. After that, 1 wt% Triton -X was added to ease the process of electrospinning into the dispersion and then 15 wt% polyvinyl alcohol (PVA) polymer was introduced to it followed by 2 h of stirring at 80 °C. Electrospinning parameters such as voltage, distance, and feed rate were optimized using design of experiments (DOE) software. Electrospun membranes were calcinated at 600 °C for 2 h with a heating rate of 0.5 °C/min (Nabertherm Co., 30–3000 °C, Germany) to remove the PVA and obtain ZnO nanofibers.

2.2 Production of Sensors

The ZnO-based sensor was made by directly placing the calcinated layer on the interdigitated Au electrode with a gap of 0.25 mm, positioned on an Al_2O_3 substrate. The schematic of the electrode employed can be seen in Fig. 1, with the sensing layer directly fixed on it.

2.3 Characterization

The behaviors of solutions used for electrospinning process were studied in viscosity (Lamy Rheology Viscometer RM100 Plus), conductivity (Mettler Toledo Seven Direct SD23), and surface tension (GBX Instrumentation Scientific 3S).

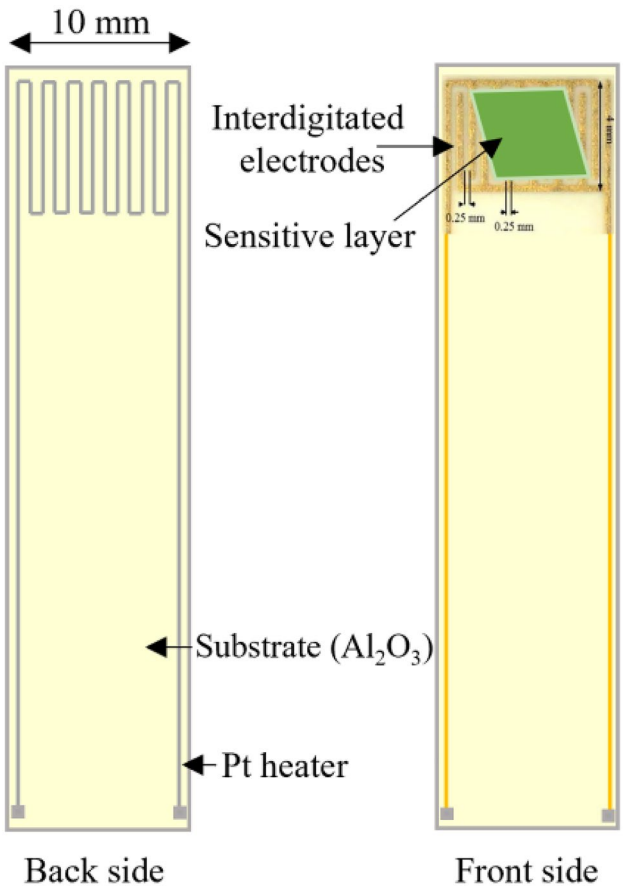

Fig. 1 The electrode used in production of the sensors

The microstructural and morphological characteristics of ZnO nanofibers were investigated by field-emission scanning electron microscope (SEM) (AIS2100, SERON), and the nanofibers' diameter was measured using Image j software. The phase and crystallinity of the samples were analyzed by X-ray diffraction (XRD) (Thermo Fisher EQUINOX 3000).

To investigate the sensing behavior of the sensors toward a particular gas, the experimental setup presented in Fig. 2 was employed. The system comprises a Teflon chamber, a bubbler in a bath for humidity control, and three mass flow meters controlled by a computer. The gas flow meter can modulate the concentration of various gases with precision. To maintain a uniform gas flow rate for all the sensors during the tests, the total flow of dry and humid air was adjusted to 1000 ml/min, and the target gas flow rate was set to 50 ml/min. Before conducting the gas sensing experiments, the sensors were initially heated to the operating temperature of the sensor in ambient air for a few days and then exposed to the specific gas under study. To ensure the resistance stability of the sensors

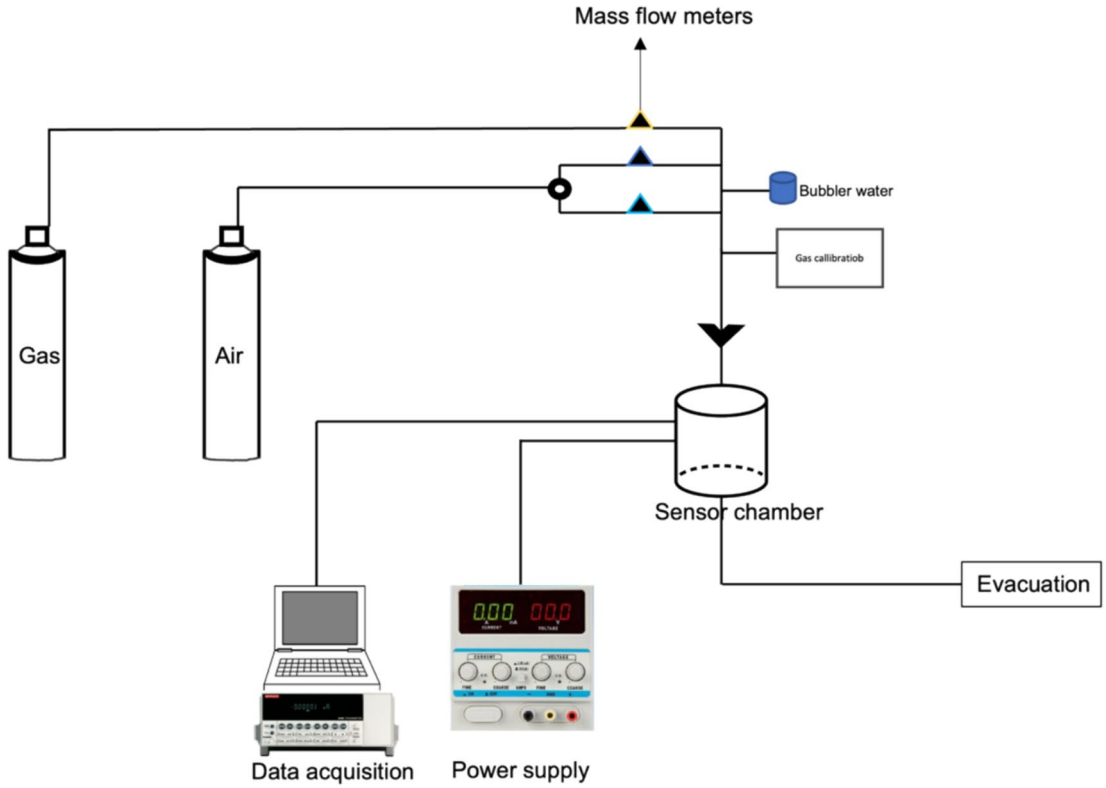

Fig. 2 The homemade sensing device schematic

before exposure to gases, a mixture of dry and humid air with controlled relative humidity was initially introduced into the Teflon chamber containing the sensors. When the electrical resistance became stable, a certified specific gas such as NO was injected at a flow rate of less than 50 ml/min, which was determined based on the gas concentration in the experiments. Finally, a data logger is employed to capture the data. To ensure precise control over the gas flow rate, a mass flow controller was used, and closely monitored.

The resistance of the sensor device was assessed using a data acquisition system (Keithley 2700). The sensor response was calculated as $(R_g\_R_a)/R_a$, where R_a represents the initial resistance and R_g is the resistance observed during the experiment. Target gas concentrations were calibrated using a commercial chemiluminescence NOx analyzer (Thermo Electron, Netherlands).

Moreover, this study also involved the calculation of both the response time and recovery time. The response time was precisely defined as the duration necessary for the sensor to attain 90% of its maximum response, while the recovery time was defined as the required period for the sensor to return to 10% of its response level during the recovery phase.

3 Results and Discussion

3.1 Electrospun Membrane Properties

To achieve the optimal electrospinning solution, measurements of viscosity, surface tension, and conductivity were conducted. The optimal conditions were obtained with the values of 2.512 ± 0.023 Pa·s, 39.23 ± 0.73 mN/m, and $10{,}130.48 \pm 33.79$ µS/cm, respectively.

To elaborate the effect of fiber diameter on the sensitivity and response of the sensors toward NO gas, three different diameters were produced by changing electrospinning parameters including voltage, feed rate, and distance in the electrospinning process, as represented in Table 1. In the end, three different diameters of 160 ± 0.042, 240 ± 0.06, and 310 ± 0.7 nm were produced after calcination labeled D-16, D-24, and D-31, respectively. Owing to the fact that all collector sizes and duration of electrospinning were the same, the thickness remained consistent in all three samples with the average of 20.25 ± 0.53.

Among other samples, D-16 demonstrated the best response to the target gas at concentrations of 1 ppm and 500 ppb (see Sect. 3.2). Therefore, the size of the collector

Table 1 Electrospinning and membrane parameters for different diameter of nanofibers

Sample	Distance (cm)	Voltage (kV)	Feed rate (ul/h)	Sensitivity after calcination (g/cm^3)	Pore area (m^2/g)	Diameter (um)	
						Before calcination	After calcination
D-16	20	18	200	0.4 ± 0.6	76.76	0.46 ± 0.1	0.16 ± 0.042
D-24	16	18	200	20.84 ± 0.5	70.35	0.55 ± 0.11	0.24 ± 0.06
D-31	22	22	300	20.12 ± 1.1	76.56	0.71 ± 0.15	0.31 ± 0.7

Table 2 Structural and sensing properties of the sensor with different thicknesses

Sample	Collector size (cm^2)	Thickness (um)		Pore area (m^2/cg)	Grain size (nm)	Density after calcination (mg/cm^3)
		Before calcination	After calcination			
T-5	5 × 5	43.0 ± 8.11	25.7 ± 3.56	33.89	14.20	0.44
T-10	10 × 10	33.9 ± 5.17	23.7 ± 5.7	52.15	14.6	0.42
T-15	15 × 15	27.2 ± 3.55	19.8 ± 5.45	70.35	14.68	0.35

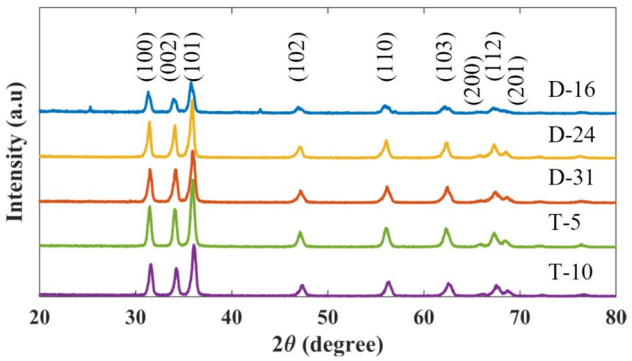

Fig. 3 XRD spectra of XRD after calcination for different ZnO fiber diameters and thicknesses

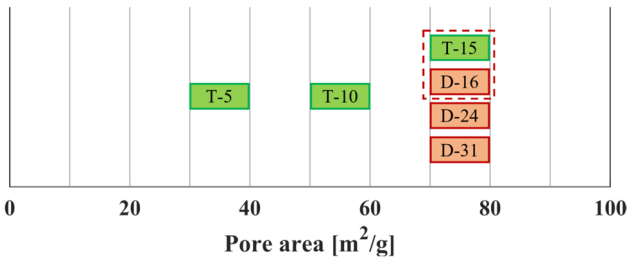

Fig. 4 The pore area range of the sensors

was altered keeping the distance, voltage, and feed rate the same as D-16, resulting in different thicknesses as represented in Table 2. Consequently, with an increase in the collector surface area, there is a corresponding reduction in the thickness of the layer. The nanofibers' diameters were measured in all three thicknesses and they had the same diameter of 160 ± 0.03 nm.

As shown in Table 2, reducing the area of the collector leads to an increase in the thickness of the nanofiber membrane. The thickness of the membrane produced via electrospinning is influenced by various factors, including solution concentration, applied voltage, flow rate, needle diameter, collector distance, and collector size [31]. In this case, since all other parameters remain constant, decreasing the size of the collector during electrospinning can result in a thicker membrane [32]. Moreover, sample D-16 had the same thickness of sample T-15.

Continuingly, the XRD spectra of calcinated ZnO nano fibers with different diameters and thicknesses are presented in Fig. 3. The results are in agreement with previous studies [33].

In Fig. 3, the XRD pattern of the ZnO powder vividly displays a number of peaks originating from (1 0 0), (0 0 2), (1 0 1), (1 0 2), (1 0 3), (2 0 0), (1 1 2), and (2 0 1) planes, which index the hexagonal wurtzite structure of ZnO well. The high intensity of the aforementioned peaks dictates the high crystallinity of ZnO powder [34, 35].

The grain size average of all samples was calculated according to Scherer's equation [34] using XRD. As it was stated in Sect. II, the thickness of D-16 was the same as sample T-15; therefore, they had the same grain size of 14.5 nm. In addition, it was seen that by increasing the diameter of the samples, the grain size experienced 1.27 nm increase whereas by thickness alteration, no significant difference was observed among the T-samples. This is particularly noteworthy, as fine grain size exhibits superior sensitivity [35].

To understand the effect of porosity, samples were analyzed by BET test. The pore area of all the samples is presented in Fig. 4. It can be seen that as the thickness rises, the surface area reaches its maximum value. Moreover,

for all the diameters, the range of the pore area remained constant.

3.2 Diameter and Sensing Performance

The SEM images presented in Fig. 5 illustrate the nanofibers both prior and post-calcination. It is noteworthy that the well-optimized nanofibers with different diameters feature a structure which is entirely free of beads and droplets, and above all, maintains a consistent and uniform formation. Following the calcination process, there is an evident reduction in the diameter of the nanofibers. This change can be attributed to the removal of the polymer. Furthermore, it is apparent that the calcination process induces a certain level of shrinkage, resulting in the creation of ZnO particles that resemble fibers. In addition, this shrinkage resulted in white spots, likely due to the collapse of nanofibers at the joints after the polymer was removed, leading to clusters of ZnO particles. Another contributing factor might be the evaporation of PVA from beads present on the web, which left these white spots behind. Moreover, in post-calcination, the long nanofibers experience a transformation into shorter segments.

The performance of metal oxide sensors, such as ZnO, in sensing is inherently influenced by the operating temperature [36]. Hence, to determine the ideal temperature, D-16 was subjected to testing across a temperature range

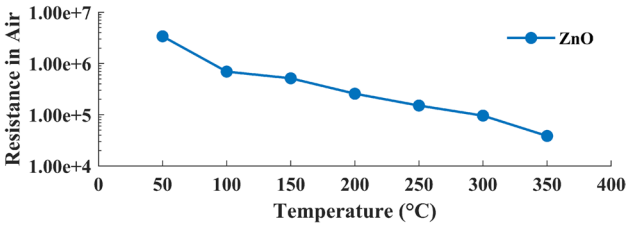

Fig. 6 Initial sensor resistance in clean air versus temperature for D-16 sensor

spanning from 50 to 350 °C, while exposed to 1 ppm concentration of NO. The reason for choosing this sample was based on previous experimental studies. As illustrated in Fig. 6, with the rise in temperature, initial resistance (Ra) decreases, signifying a shift toward semiconducting behavior. This phenomenon occurs due to an increased number of electrons transitioning into the conduction band (CB) of ZnO as the temperature increases [37].

As depicted in Fig. 7, the sensor (D-16) exhibited its interestingly highest response of 35.57 at the temperature of 200 °C. Consequently, this specific temperature was selected for further investigation. As the temperature increases, the response of the sensor to 1 ppm NO decreases. This effect may be due to changes in the kinetic energy at the surface. At higher temperatures, the adsorption and desorption of the gas occur too quickly for

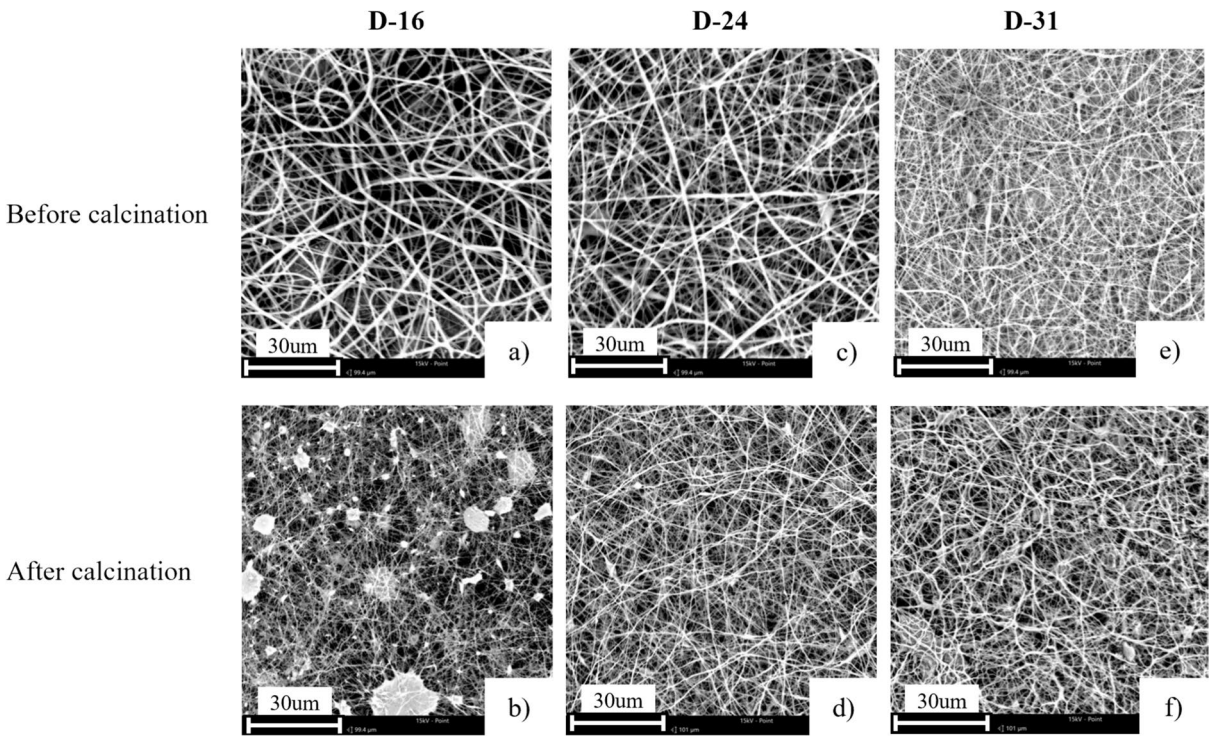

Fig. 5 SEM images of nanofibers before calcination (**a**–**c**) and after calcination (**d**–**f**) with regard to different diameters

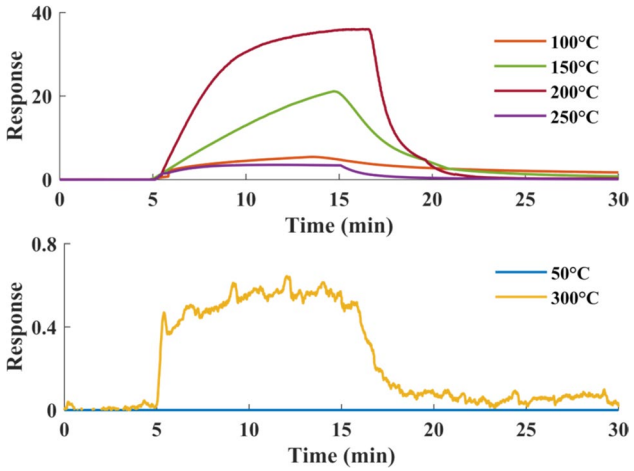

Fig. 7 Dynamic response curve for D-16 sensor in different temperature (50–300 °C) toward 1 ppm of NO

detection, causing some of the adsorbed NO molecules to desorb before being recognized.

Following the initial test, the sensors with three different diameters (D-16, D-24, D-31) were subsequently evaluated in the presence of 1 ppm and 500 ppb of NO gas at the temperature of 200 °C. First of all, as it is demonstrated in Fig. 8a, increasing the gas concentration results in increasing in the response, it can be because more gas molecules are in contact with the surface of the layer [38]. Moreover, increase in ZnO nanofiber diameter leads to response decrease toward the gas, depicted in Fig. 8b. The specific surface area likely plays a pivotal role in accounting for the distinct response behaviors exhibited by the ZnO nanofibers [22]. Nanofibers with small diameters can enhance the sensitivity of a ZnO gas sensor. This is because a smaller diameter increases the surface area and the number of active sites for gas adsorption and reaction. It also reduces the grain size and grain boundary resistance of ZnO, improving the electrical conductivity and gas sensing mechanism of the sensor [39]. As observed, D-31 exhibits the lowest response to the target gas (Fig. 9), possibly due to its larger crystal size (as presented in Fig. 3). In comparing the sensors, there is less difference in response between D-16 and D-24, and this can be because of the white spots created in the D-16 membrane. These white regions are able to reduce the sensitivity of the sensor as they act as a short circuit, allowing charge carriers to bypass them. As a result, when gas molecules adsorb onto these areas, no change in resistivity is detected.

Furthermore, response/recovery time for D-16 sensor at 500 ppb of NO was 358 and 191 s, respectively (Fig. 9).

3.3 Thickness and Sensing Performance

The SEM images of different thicknesses are shown in Fig. 10. As depicted in the SEM images, when viewed from the side, all the samples exhibit nanofibers uniformly positioned on top of each other, forming a nonwoven structure. This specific structure results in the creation of significant porosity within the membrane which can play a crucial role in enhancing the sensitivity of gas sensors based on nanofibers compared to other film generating techniques [14].

By increasing the thickness, more material was collected on the specific surface area thus, with respect to thickness of the samples and the following equation, the density can be calculated (Eq. (1)).

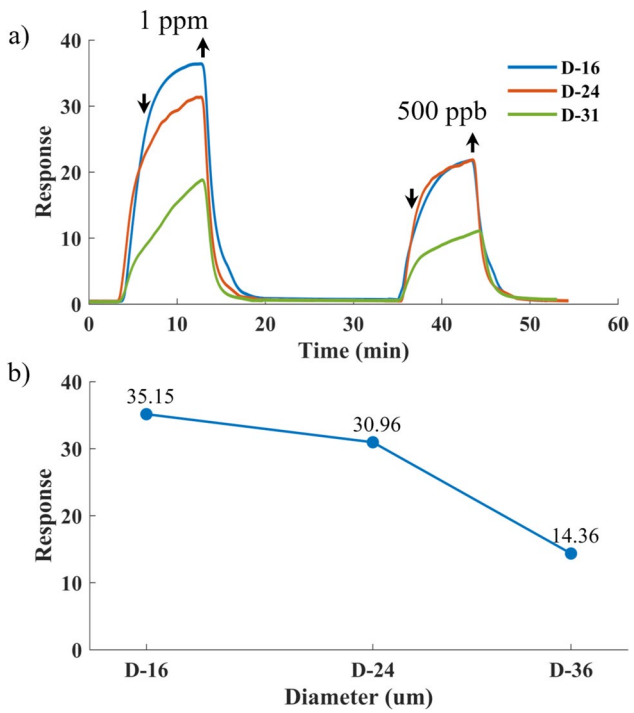

Fig. 8 **a** The dynamic response of NO in different diameters, and **b** the maximum response of NO toward 1 ppm in different diameters

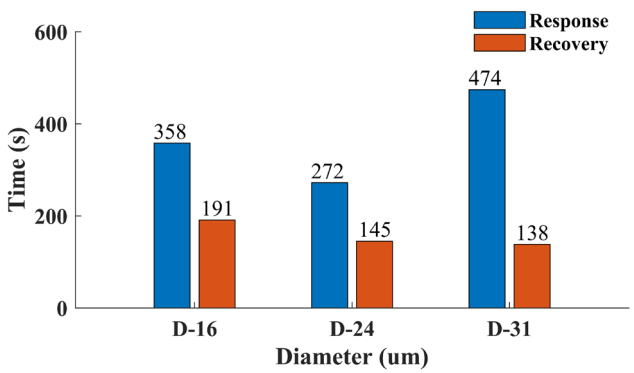

Fig. 9 Response as the function of response/recovery time for three different diameters at 500 ppb

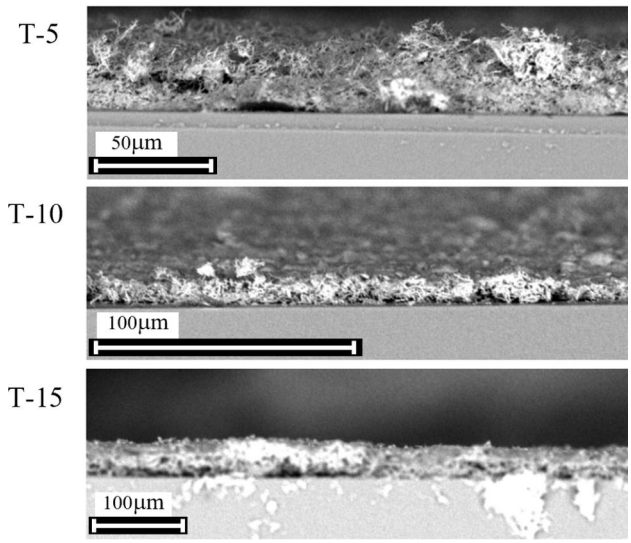

Fig. 10 The SEM images for different thickness of membrane of as-spun ZnO from side view

$$\rho = m/V \tag{1}$$

where ρ is density, m is weight, and V is sample volume.

Here, the density for T-10 is the most which causes lower resistance. Henceforth, the initial resistance for higher density material is less as the current passes through more easily. It is in accordance with the dynamic curve of resistance–time of thickness, as shown in Fig. 11.

The typical dynamic transient responses of the produced sensors at two different concentrations (1 ppm and 500 ppb) at 200 °C and the linear relation between the responses and thickness is plotted in Fig. 12a, b, respectively. As observed, the sensor with the least thickness exhibits the best sensing performance, having the highest sensitivity at 45.74 and 21.33 toward 1 ppm and 500 ppb of NO, respectively. Importantly, when the thickness is reduced, the crystal size remains almost constant while the pore area decreases as the thickness increases, as shown in Fig. 4. Therefore, the lowest response can be due to the lowest porosity in T-5 which has the highest thickness.

Moreover, the response and recovery time for all three thicknesses are shown in Fig. 13. When the gas is injected, penetration to the layers may not be as easy as thinner substrate, so the bottom of the layer probably cannot be reached by the gas during injecting; thus, the resistance does not change.

Notably, it is observed that by increasing the thickness, recovery time reduces. According to previous studies, the response time and recovery time depend on several factors, such as the gas concentration, the operating temperature, the morphology and structure of the sensing material, and the thickness of the sensing layer [40]. The decrease in response time due to the thicker sensor can be attributed to the fact that gas molecules must diffuse through a greater thickness of the sensing material to reach the surface and interact with the adsorbed oxygen ions. This diffusion process may not happen completely, and the gas molecules could not penetrate to the substrate, this can lead to a decrease in the recovery time. When the sensor is removed from the target gas, the gas molecules must diffuse back from the surface to the bulk of the sensing material. This process is inherently faster, thus aiding in the quicker recovery of the sensor [41].

According to the results, the sensor labeled as D-16 and T-15, with the smallest diameter and thickness, exhibited the highest response to 1 ppm and 500 ppb of NO gas at 200 °C. Apart from sensitivity, stability and selectivity of the sensor are of great importance to its applicability. In addition, the sensors were also tested in 70% and 90% humidity and their response reduced to a little above half of when subjected to 50% humidity, in 90% humidity. Finally, selectivity and repeatability of the sensors were

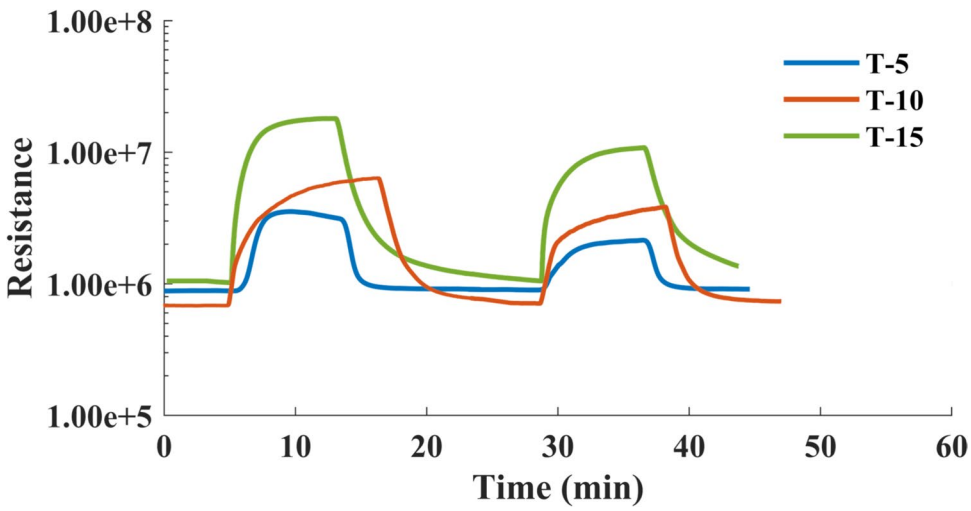

Fig. 11 Dynamic resistance–time curves for samples with different thicknesses to 1 ppm and 500 ppb NO at 200 °C

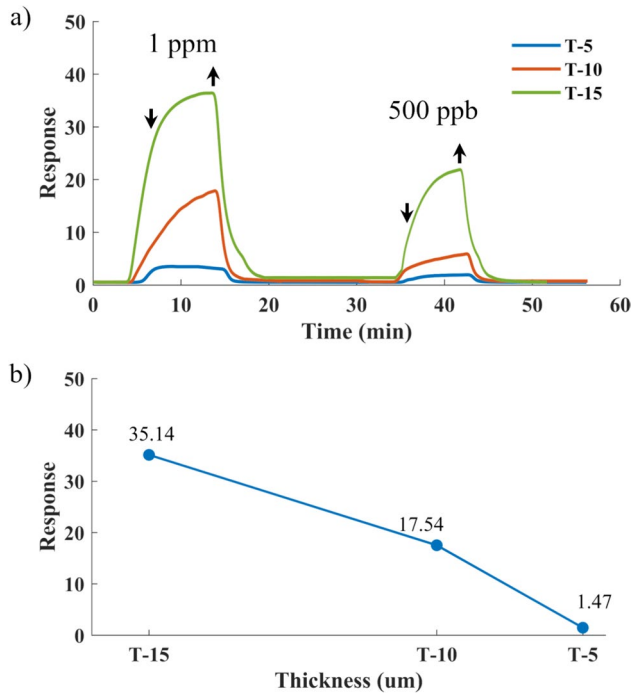

Fig. 12 **a)** The dynamic response of NO in different thicknesses, and **b)** The maximum response of NO toward 1 ppm in different thicknesses at 200 °C

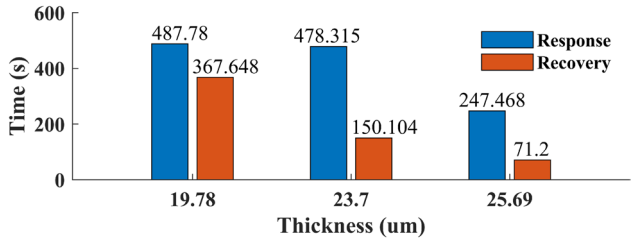

Fig. 13 Response as the function of response/recovery time for three different thicknesses at 500 ppb

evaluated. Figure 14a shows the selectivity graph of the sensor for NO, ethanol, isopropanol, and acetone. Target gases preparation followed a specific protocol. NO gas, at concentrations of 100 ppm in a nitrogen (N_2) atmosphere, was utilized. Volatile organic compounds (VOCs), used aqueous solutions following Henry's law at 25 °C. The measurements were performed under the same conditions, with 10 min of exposure to the respective gases and 20 min of recovery time. The sensor response for NO gas is about 84 times greater than for the other gases. This demonstrates that the sensor is NO selective. Repetitive sensing tests for five reversible cycles for 500 ppb of NO were carried out at 200 °C, as shown in Fig. 14b. It is observed that the sensors responded ($(R_g - R_a/R_g)*100) = 22.95$) instantly after the test molecules were introduced and

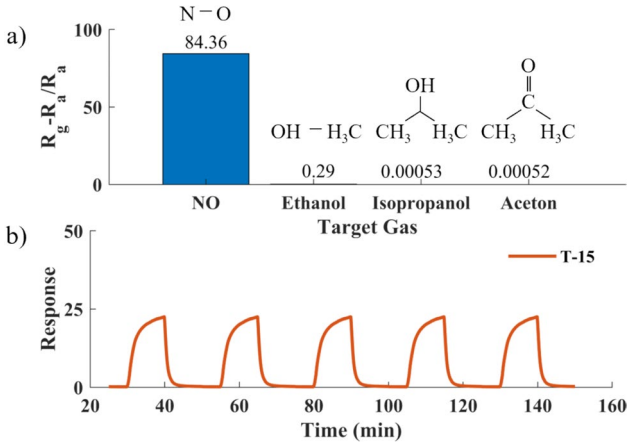

Fig. 14 **a** Response as function of selectivity and **b** repeatability of the sensor for NO at 500 ppb

rapidly returned to their initial state when exposed to air. In addition, after five cycles of continuous testing, the sensors exhibited fairly stable response values, indicating its good stability.

The relationship between electrospinning parameters and sensing performance can be better understood through comparison with recent literature. While our D-16 sample achieved optimal sensing performance with 160 nm diameter fibers, this aligns with Wang et al.'s findings [42] where they demonstrated that controlling fiber diameter below 200 nm creates optimal surface-to-volume ratios for gas molecule interactions. Similar to their work, we observed that smaller diameter fibers provide more accessible active sites for gas adsorption.

Our optimization of electrospinning parameters (voltage: 18 kV, distance: 20 cm, feed rate: 200 µL/h) resulted in uniform fiber formation without beading, comparable to results reported by Wang et al. [43]. However, our work extends beyond mere morphological control by demonstrating how these parameters directly influence sensing performance. The enhanced sensitivity (25 Ω/Ω) achieved in our thinner membranes can be attributed to the optimized porosity and interconnected fiber network structure, which facilitates efficient gas diffusion pathways.

The impact of fiber diameter on sensing performance can be contextualized with existing literature:

- Our 160 nm fibers demonstrated 96% higher sensitivity compared to 310 nm fibers.
- The faster recovery time (191 s) in smaller diameter fibers aligns with recent findings about surface reaction kinetics in nanostructured metal oxides.

Regarding thickness optimization:

- Our finding that thinner membranes (19 µm) outperform thicker ones correlates with recent theoretical models of gas diffusion in porous networks.
- The observed twofold improvement in gas sensitivity with thickness reduction provides quantitative support for the importance of optimizing layer thickness.
- The relationship between thickness and response time shows similar trends to those reported in recent literature, though our optimization achieves faster recovery times.

These comparisons demonstrate that while our fabrication approach builds on established principles, the systematic optimization of both diameter and thickness parameters achieves superior sensing performance. The interconnected effects of these parameters on sensor response and recovery times provide new insights for designing high-performance gas sensors.

3.4 Gas Sensing Mechanism

The most widely accepted explanation of the NO sensing mechanism in ZnO, an n-type semiconductor, involves a reaction occurring at the gas–solid interface (Fig. 15). When a ZnO gas sensor is exposed to air at 200 °C, the free electrons from the conduction band are captured by the adsorbed oxygen atoms, forming adsorbed oxygen anions (O_2^-, O^-). This interaction in ZnO creates an electron depletion layer, leading to an increase in resistance. Upon exposure to NO, NO molecules adhere to the ZnO surface and react with the adsorbed O_2^- and O^- anions at the ZnO grain boundaries and the O_2^- disappears rapidly. Conclusively, more electrons are captured from the conduction band, causing an increase in resistance once again.

The oxygen species capture conduction electrons from the materials, which leads to a decrease in the electron concentration. Once the oxidizing gas NO was introduced into the testing chamber, as in Fig. 15, NO molecules will be absorbed on the ZnO surface. Electrons can be extracted from the conduction band of ZnO, leading to the rise of the resistance [44]. The corresponding possible reactions are described in Eqs. (2), (3), and (4) [45].

$$NO_{(gas)} + e^- \leftrightarrow NO_{(ads)} \tag{2}$$

$$NO_{(ads)} + e^- \leftrightarrow NO^- \tag{3}$$

$$NO_{(gas)} + O_{2\,(ads)} + e^- \leftrightarrow NO_{2\,(ads)} + O_{(ads)} \tag{4}$$

When a thin ZnO film with small diameter of nanofiber consisting of fine grains is exposed to air, the depletion layer would extend throughout the entire layer of ZnO film, and its resistance becomes extremely large. In an NO environment, the depleted layer will widen quickly as the gas takes more electron from the conduction band of ZnO-adsorbed oxygen reaction, and the resistance of the ZnO film would experience a large change. As it is depicted in Fig. 16, after being exposed to air or NO, due to the many channels formed in the ZnO-based nanofibers membrane, the gas could freely enter the inner parts of the sensing layer, resulting in an almost-complete depletion of the electrons of the whole ZnO membrane.

The ZnO sensor results emphasize the importance of these findings and suggest strong potential for future advancements in gas sensor technology, with the goal of achieving a more consistent and high-performance sensing capability relative to prior studies summarized in Table 3.

As observed in Table 1, the ZnO sensor presented in this study was of the lowest concentration of ppm, 5 ppm, the

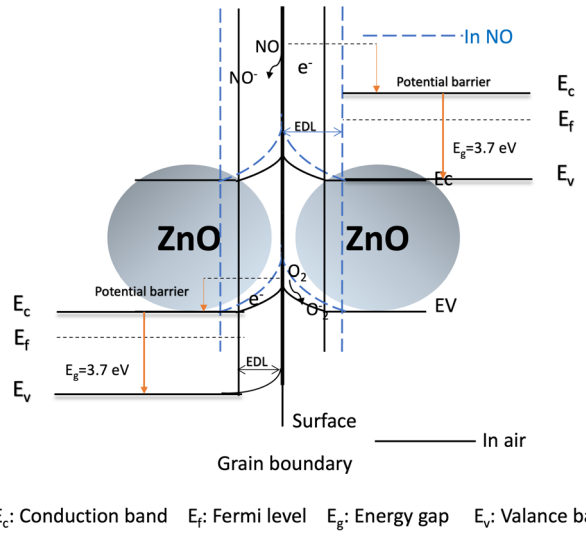

Fig. 15 Schematic of the proposed NO sensing mechanism of ZnO with band diagram ZnO in air and in NO

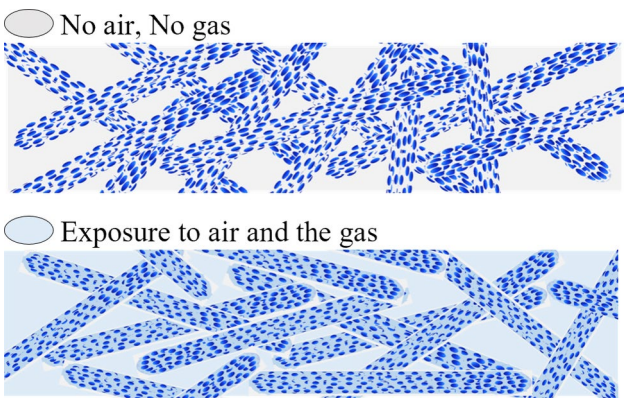

Fig. 16 Thin membrane consisting of grain in a format of nanofibers

Table 3 Previous research on electrospun ZnO-based gas sensors toward NO

SMO	Precursor	Target gas concentration (ppm)	Temperature (°C)	Response (R_g/R_a)	Ref
ZnO	ZnAc:PVA = 0.5	NO 12	200	7	[46]
ZnO/CdO	ZnAc:PVA = 0.55	NO 33	200	22.6	[47]
Au-Polyaniline/ZnO	ZnAc:PVA = 0.7	NO_2 50	350	50	[37]
Tb_2O_3/ZnO	ZnAc:PvP	NO 1	180	28.3	[48]
ZnO nanofibers	**ZnAc:PVA = 1.5**	**NO 5 and 0.5**	**200**	**84 and 25**	**This study**

Bold indicates the results of the present study

lowest temperature among available ZnO sensors, 200 °C, and the high response of 84 to NO gas.

4 Conclusion and Perspectives

In conclusion, this study demonstrates the successful synthesis of ZnO nanofibers with varied diameters and thicknesses through the electrospinning method. The resulting gas sensors exhibit promising sensing performance, particularly the sensors with thinner membranes and smaller diameters. At the optimal operating temperature of 200 °C, these sensors display an exceptional response magnitude of 20 when exposed to 500 ppb of NO gas concentration, surpassing previously reported results. In a nutshell:

- Controlling the structural properties of nanofibers to have the capability of reproducibility the sensing layer
- Increasing 30% of the membrane thickness leads to decrease the sensitivity by 96% regarding to reduction in pore area
- Decreasing 90% of the nanofiber diameter enhances the sensitivity to NO gas by two times

The research contributes to the understanding of the sensing mechanism by incorporating an energy band diagram, providing insights into the underlying processes. The findings underscore the importance of adjusting electrospinning parameters to optimize ZnO nanofiber structures to enhance NO gas detection, addressing a critical need for cost-effective and efficient gas sensors in both industrial and biomedical applications.

Acknowledgements This research project receives financial support from Région Hauts de France. This work is based upon research funded by Iran National Science Foundation (INSF) under project No.4020210.

Author contributions Niloufar Khomarloo: writing—original draft, visualization. Roohollah Bagherzadeh: review, supervision, and data validation. Hayriye Gidik: review, supervision, and data validation. Elham Mohsenzadeh: review, supervision, and data validation. Masoud Latifi: review and supervision. Marc Debliquy: supervision and data validation. Ahmadou Ly: technical support. Driss Lahem: supervision.

Funding This work was funded by Iran National Science Foundation, 4020210, Roohollah Bagherzadeh.

Data availability The data that support the findings of this study are available from the corresponding author upon reasonable request.

Declarations

Conflict of interest There are no conflicts to declare.

References

1. N. Huang, Y. Cheng, H. Li, L. Zhao, Z. He, C. Zhao, F. Liu, L. Ding, Selective-detection NO at room temperature on porous ZnO nanostructure by solid-state synthesis method. J. Colloid Interface Sci. **556**, 640–649 (2019)
2. D. Hashoul, H. Haick, Sensors for detecting pulmonary diseases from exhaled breath. Eur. Respir. Rev. **28**(152), 190011 (2019)
3. O. Lawal, W.M. Ahmed, T.M. Nijsen, R. Goodacre, S.J. Fowler, Exhaled breath analysis: a review of 'breath-taking' methods for off-line analysis. Metabolomics **13**, 1–16 (2017)
4. Z. Ma, K. Yang, C. Xiao, L. Jia, Electrospun Bi-doped SnO2 porous nanosheets for highly sensitive nitric oxide detection. J. Hazard. Mater. **416**, 126118 (2021)
5. G. Korotcenkov, The role of morphology and crystallographic structure of metal oxides in response of conductometric-type gas sensors. Mater. Sci. Eng. R. Rep. **61**(1–6), 1–39 (2008)
6. H.A. Khorami, M. Keyanpour-Rad, M.R. Vaezi, Synthesis of SnO2/ZnO composite nanofibers by electrospinning method and study of its ethanol sensing properties. Appl. Surf. Sci. **257**(18), 7988–7992 (2011)
7. F. Li, Y. Chen, J. Ma, Porous SnO2 nanoplates for highly sensitive NO detection. J. Mater. Chem. A **2**(20), 7175–7178 (2014)
8. J. Moon, J.A. Park, S.J. Lee, T. Zyung, Semiconducting ZnO nanofibers as gas sensors and gas response improvement by SnO2 coating. ETRI J. **31**(6), 636–641 (2009)
9. I.-D. Kim, E.-K. Jeon, S.-H. Choi, D.-K. Choi, H.L. Tuller, Electrospun SnO2 nanofiber mats with thermo-compression step for gas sensing applications. J. Electroceram. **25**, 159–167 (2010)
10. F. Gu, R. Nie, D. Han, Z. Wang, In2O3–graphene nanocomposite based gas sensor for selective detection of NO2 at room temperature. Sens. Actuators B Chem. **219**, 94–99 (2015)
11. C.-Y. Lin, Y.-Y. Fang, C.-W. Lin, J.J. Tunney, K.-C. Ho, Fabrication of NOx gas sensors using In2O3–ZnO composite films. Sens. Actuators B Chem. **146**(1), 28–34 (2010)
12. H. Wu, K. Kan, L. Wang, G. Zhang, Y. Yang, H. Li, L. Jing, P. Shen, L. Li, K. Shi, Electrospinning of mesoporous p-type In2O3/TiO2 composite nanofibers for enhancing NOx gas sensing properties at room temperature. CrystEngComm **16**(38), 9116–9124 (2014)

13. V.T. Duoc, C.M. Hung, H. Nguyen, N. Van Duy, N. Van Hieu, N.D. Hoa, Room temperature highly toxic NO2 gas sensors based on rootstock/scion nanowires of SnO2/ZnO, ZnO/SnO2, SnO2/SnO2 and ZnO/ZnO. Sens. Actuators B Chem. **348**, 130652 (2021)
14. J.-H. Kim, A. Mirzaei, H.W. Kim, P. Wu, S.S. Kim, Design of supersensitive and selective ZnO-nanofiber-based sensors for H2 gas sensing by electron-beam irradiation. Sens. Actuators B Chem. **293**, 210–223 (2019)
15. P. Singh, L.-L. Hu, H.-W. Zan, T.-Y. Tseng, Highly sensitive nitric oxide gas sensor based on ZnO-nanorods vertical resistor operated at room temperature. Nanotechnology **30**(9), 095501 (2019)
16. J. Xuan, G. Zhao, M. Sun, F. Jia, X. Wang, T. Zhou, G. Yin, B. Liu, Low-temperature operating ZnO-based NO2 sensors: A review. RSC Adv. **10**(65), 39786–39807 (2020)
17. X. Tian, X. Cui, T. Lai, J. Ren, Z. Yang, M. Xiao, B. Wang, X. Xiao, Y. Wang, Gas sensors based on TiO2 nanostructured materials for the detection of hazardous gases: A review. Nano Materials Science **3**(4), 390–403 (2021)
18. L.A. Mercante, R.S. Andre, L.H. Mattoso, D.S. Correa, Electrospun ceramic nanofibers and hybrid-nanofiber composites for gas sensing. ACS Appl. Nano Mater. **2**(7), 4026–4042 (2019)
19. W. Wang, H. Huang, Z. Li, H. Zhang, Y. Wang, W. Zheng, C. Wang, Zinc oxide nanofiber gas sensors via electrospinning. J. Am. Ceram. Soc. **91**(11), 3817–3819 (2008)
20. V. Esposito, D. Marani, *Metal Oxide-Based Nanofibers and Their Applications* (Elsevier, 2021)
21. S.-H. Hwang, Y.K. Kim, S.H. Hong, S.K. Lim, Cu/CuO@ ZnO hollow nanofiber gas sensor: Effect of hollow nanofiber structure and P-N junction on operating temperature and sensitivity. Sensors **19**(14), 3151 (2019)
22. A. Katoch, Z.U. Abideen, J.-H. Kim, S.S. Kim, Influence of hollowness variation on the gas-sensing properties of ZnO hollow nanofibers. Sens. Actuators B Chem. **232**, 698–704 (2016)
23. S. Wei, M. Zhou, W. Du, Improved acetone sensing properties of ZnO hollow nanofibers by single capillary electrospinning. Sens. Actuators B Chem. **160**(1), 753–759 (2011)
24. L. Guo, Z. Yang, Y. Li, B. Zu, X. Dou, Sensitive, real-time and anti-interfering detection of nitro-explosive vapors realized by ZnO/rGO core/shell micro-Schottky junction. Sens. Actuators B Chem. **239**, 286–294 (2017)
25. Y. Fan, L. Kang, W. Zhou, W. Jiang, L. Wang, A. Kawasaki, Control of doping by matrix in few-layer graphene/metal oxide composites with highly enhanced electrical conductivity. Carbon **81**, 83–90 (2015)
26. S.-H. Choi, G. Ankonina, D.-Y. Youn, S.-G. Oh, J.-M. Hong, A. Rothschild, I.-D. Kim, Hollow ZnO nanofibers fabricated using electrospun polymer templates and their electronic transport properties. ACS Nano **3**(9), 2623–2631 (2009)
27. A. Aziz, N. Tiwale, S.A. Hodge, S.J. Attwood, G. Divitini, M.E. Welland, Core–shell electrospun polycrystalline ZnO nanofibers for ultra-sensitive NO2 gas sensing. ACS Appl. Mater. Interfaces **10**(50), 43817–43823 (2018)
28. A. Hassan, J. Greenway, A. Ray, A. Nabok, In situ optical study of ozone interaction with polyphenylsulfide thin films. J. Phys. D Appl. Phys. **36**(17), 2130 (2003)
29. Y. Shimizu, N. Kuwano, T. Hyodo, M. Egashira, High H2 sensing performance of anodically oxidized TiO2 film contacted with Pd. Sens. Actuators B Chem. **83**(1–3), 195–201 (2002)
30. S. Saukko, V. Lantto, Influence of electrode material on properties of SnO2-based gas sensor. Thin Solid Films **436**(1), 137–140 (2003)
31. H. Thillaipandian, P. Pitchaimuthu, D. Chandrasekaran, G.D.V. Rengaswami, Recent developments in electrospinning spinneret and collector assembly for biomedical applications, in *Electrospun Polymeric Nanofibers: Insight into Fabrication Techniques and Biomedical Applications*. ed. by R. Jayakumar (Springer, Cham, 2022), pp.1–21
32. S. Han, K. Nie, J. Li, Q. Sun, X. Wang, X. Li, Q. Li, 3D electrospun nanofiber-based scaffolds: From preparations and properties to tissue regeneration applications. Stem Cells Int. **2021**(1), 8790143 (2021)
33. K. Thangavel, T. Roshini, V. Balaprakash, P. Gowrisankar, S. Sudha, M. Mohan, Structural, morphological and antibacterial properties of ZnO nanofibers fabricated by electrospinning technique. Mater. Today Proc. **33**, 2160–2166 (2020)
34. R. Dhahri, M. Hjiri, L. El Mir, E. Fazio, F. Neri, F. Barreca, N. Donato, A. Bonavita, S.G. Leonardi, G. Neri, ZnO: Ca nanopowders with enhanced CO2 sensing properties. J. Phys. D Appl. Phys. **48**(25), 255503 (2015)
35. A. Katoch, G.-J. Sun, S.-W. Choi, J.-H. Byun, S.S. Kim, Competitive influence of grain size and crystallinity on gas sensing performances of ZnO nanofibers. Sens. Actuators B Chem. **185**, 411–416 (2013)
36. S. Das, S. Roy, T.S. Bhattacharya, C.K. Sarkar, Efficient room temperature hydrogen gas sensor using ZnO nanoparticles-reduced graphene oxide nanohybrid. IEEE Sens. J. **21**(2), 1264–1272 (2020)
37. M. Bonyani, S.M. Zebarjad, K. Janghorban, J.-Y. Kim, H.W. Kim, S.S. Kim, Au sputter-deposited ZnO nanofibers with enhanced NO2 gas response. Sens. Actuators B Chem. **372**, 132636 (2022)
38. S.R. Vanga, V. Sarada, Improving sensitivity of ZnO nanorods for the application of gas sensors at low temperatures: a review, in *2022 Second International Conference on Next Generation Intelligent Systems (ICNGIS)*. (IEEE, 2022), pp.1–6
39. S.-W. Choi, J.Y. Park, S.S. Kim, Dependence of gas sensing properties in ZnO nanofibers on size and crystallinity of nanograins. J. Mater. Res. **26**, 1662–1665 (2011)
40. A. Ponzoni, A statistical analysis of response and recovery times: the case of ethanol chemiresistors based on pure SnO2. Sensors **22**(17), 6346 (2022)
41. D.Y. Nadargi, A. Umar, J.D. Nadargi, S.A. Lokare, S. Akbar, I.S. Mulla, S.S. Suryavanshi, N.L. Bhandari, M.G. Chaskar, Gas sensors and factors influencing sensing mechanism with a special focus on MOS sensors. J. Mater. Sci. **58**(2), 559–582 (2023)
42. Y. Wang, Y. Xu, W. Zhai, Z. Zhang, Y. Liu, S. Cheng, H. Zhang, In-situ growth of robust superlubricated nano-skin on electrospun nanofibers for post-operative adhesion prevention. Nat. Commun. **13**(1), 5056 (2022)
43. Y. Wang, W. Zhai, J. Li, H. Liu, C. Li, J. Li, Friction behavior of biodegradable electrospun polyester nanofibrous membranes. Tribol. Int. (2023). https://doi.org/10.1016/j.triboint.2023.108891
44. M. Kaur, S. Kailasaganapathi, N. Ramgir, N. Datta, S. Kumar, A. Debnath, D. Aswal, S. Gupta, Gas dependent sensing mechanism in ZnO nanobelt sensor. Appl. Surf. Sci. **394**, 258–266 (2017)
45. G. Murali, M. Reddeppa, C. Seshendra Reddy, S. Park, T. Chandrakalavathi, M.D. Kim, I. In, Enhancing the charge carrier separation and transport via nitrogen-doped graphene quantum dot-TiO2 nanoplate hybrid structure for an efficient NO gas sensor. ACS Appl. Mater. Interfaces **12**(11), 13428–13436 (2020)
46. O.-K. Kim, H. Kim, D. Kim, Electrospun non-directional zinc oxide nanofibers as nitrogen monoxide gas sensor. Korean J. Mater. Res. **22**(11), 609–614 (2012)
47. H. Naderi, S. Hajati, M. Ghaedi, J. Espinos, Highly selective few-ppm NO gas-sensing based on necklace-like nanofibers of ZnO/CdO nn type I heterojunction. Sens. Actuators B Chem. **297**, 126774 (2019)

48. T. Wei, W. Li, J. Zhang, X. Xie, Synthesis of Tb2O3/ZnO composite nanofibers via electrospinning as chemiresistive gas sensor for detecting NO gas. J. Alloys Compd. **947**, 169651 (2023). https://doi.org/10.1016/j.jallcom.2023.169651